Available online at www.sciencedirect.com
SCIENCE DIRECT®
ELSEVIER
International Journal of Solids and Structures 43 (2006) 5370–5385
INTERNATIONAL JOURNAL OF SOLIDS and STRUCTURES
www.elsevier.com/locate/ijsolstr

Development of a smart composite pipe joint integrated with piezoelectric layers under tensile loading

Jinquan Cheng [a,b,*], Xiaoxia Wu [b], Guoqiang Li [a], Farid Taheri [b], Su-Seng Pang [a]

[a] Department of Mechanical Engineering, Louisiana State University, Baton Rouge, LA 70803, USA
[b] Department of Civil Engineering, Dalhousie University, 1360 Barrington Street, Halifax, NS, Canada B3J 1Z1

Received 27 April 2005; received in revised form 30 December 2005
Available online 7 February 2006

Abstract

To actively reduce the stress concentration effect in adhesive layers, a novel smart adhesively bonded composite pipe joint system was developed by integrating piezoelectric layers as sensor/actuator in the connection coupler. In the presently developed smart pipe joint system, the mechanical loading induced structural deformation can be detected and monitored by integrated sensing piezoelectric layers, and then the signal is fed back to the integrated actuating piezoelectric layers to adaptively produce additional forces and moments so as to decrease the maximum peel and shear stresses in the adhesive layer. In order to theoretically predict the efficiency of the developed smart pipe joint system, an electro-mechanical theoretical analytical model was established to investigate the characteristics of the joint system under end tension load in terms of first-order shear deformation theory. Simultaneously, the state-space method was utilized to deduce the final analytical solutions, including the peel and shear stress distributions in the adhesive layer. Finally, some detailed numerical results were obtained to demonstrate the optimal design method of such smart pipe joint system and further validate the integrity of this joint system.

Keywords: Adhesive; Pipe joint; Smart structure; Piezoelectric

1. Introduction

Recently, due to the advance in adhesive material performance and the progress in the techniques of adhesive bonding, various kinds of adhesively boned joint systems have been widely applied in engineering structures, such as single-lap and double-lap joint and pipe joints in aeronautics, automotive and civil applications. Especially for the offshore gas and oil exploration and transport, adhesive-bonded pipeline networks, involving adhesive-bonded socket, butt-and-strap and flanged joints etc., are regarded as one of the most efficient and important methods. Nevertheless for any kind of adhesively bonded joint systems, the stress transfer in

* Corresponding author.
E-mail address: hitcjq@hotmail.com (J. Cheng).

0020-7683/$ - see front matter © 2006 Elsevier Ltd. All rights reserved.
doi:10.1016/j.ijsolstr.2006.01.001

the joint system is generally through the adhesive layer line via peel and shear stresses. Peel and shear stress concentrations always exist in the edge region of the adhesive layer (Goland and Reissner, 1944; Hart-Smith, 1973; Adams and Wake, 1984). Therefore, how to comprehensively study the stress distribution in the edge region and desirably improve the strength capacity of such joint is of importance for further application and reliability of this system in the more and more extensive application of the adhesive joint under some various extreme working loads. Unlike the adhesively bonded beam and plate joint systems, which have been investigated by many theoretical, numerical and experimental works, only a few studies have been conducted to investigate the adhesive-bonded pipe joint system (see Adams and Peppiatt, 1977; Chon, 1982; Chen and Cheng, 1992a,b; Choi and Lee, 1997; Lee and Oh, 1999; Yang, 2000; Yang et al., 2002; Pugno and Carpinteri, 2003). Obviously, how to improve the strength capacity of such joint systems is subsequently the most desired aim for their engineering applications. Some traditional preventive enhancement methods, such as rounding off the sharp edges, spewing fillets and tapering of the adherends etc. (Hart-smith, 1983; Roberts, 1989; Cheng et al., 1991), have been successfully applied in the engineering structures. And, some other mechanical stiffening methods have also been applied to the strength improvement of such joint. For instance, Albat and Romilly (1999) ever used the some of reinforcing patches to reduce the stresses concentration effect in adhesives. However, all of these strength enhancement methods, i.e. traditional geometric improvement or mechanical stiffening methods, are passive enhancement methods, which cannot enhance the strength of such joint system when they are subjected to sudden and extreme loading.

With the advance of smart materials performance and their processing technology, smart materials have been successfully applied as sensors and actuators in the engineering structures (Crawley and de Luis, 1987; Lee and Moon, 1990; Cheng et al., 2000; Wu et al., 2001; Batra and Geng, 2001; Luo and Tong, 2002; Cheng et al., 2005a,b). In order to adaptively improve joint systems, Cheng and Taheri have recently employed the piezoelectric smart materials to successfully improve adhesively bonded beam-like joint systems, and then introduced the adaptive strength improvement method to the common adhesively bonded joint system (Cheng and Taheri, 2005, 2006). From the previous analyses about the smart single-lap joint system integrated with the piezoelectric patches, we found that the stress concentration in the adhesive layer can be remarkably reduced through actively adjusting the electric field applied in the integrated piezoelectric patches. The purpose of this paper is to extend the application of the piezoelectric materials to adhesively bonded composite pipe joint in pipeline systems in order to construct the smart adhesively bonded pipe joint system for the reduction of stress concentrations.

In this paper, we first constructed an idealized smart adhesively bonded composite pipe joint system with the smart joint connection coupler integrated by piezoelectric layers. In order to analyze the efficiency of the integrated piezoelectric layers in the developed smart adhesively bonded pipe joint system, an electro-mechanical coupling theoretical analysis model was established to carry out the detailed theoretical investigation using first-order shear deformation theory. Further, the state-space method was adopted to present the final numerical solutions for the peel and shear stress distribution in the adhesive layer under the coupled electro-mechanical loading. Finally, some detailed simulations about the effect of stacking sequence and size of the integrated piezoelectric layers on the developed smart pipe joint system were presented in order to optimize the pipe joint system as well as the applied electric field.

2. Construction of a smart composite pipe integrated with the piezoelectric layers

It is well-known that most of the adhesively bonded pipe joints used in engineering, such as adhesively bonded socket joints, butt-and-strap joints and heat activated coupling joints etc., can be basically regarded as two pieces of composite pipes joined by a connection coupler via an adhesive layer, as shown in Fig. 1. Therefore, a common adhesively bonded pipe joint can be practically and theoretically considered to be composed of two main pipes, a connection coupler and an adhesive layer, as shown in Fig. 2. For identical material properties and geometries of such joint, the single-strap joint is a strictly symmetric structure, which would be used to simplify the future theoretical model analysis. As mentioned above, all of the experimental and theoretical works have confirmed that the peel/shear stress concentration always exists in the adhesive layer of such joint. Therefore, in order to reduce the stress concentration influence on the joint system, we proposed to develop a novel smart adhesively bonded composite pipe joint system by using the smart piezoelectric

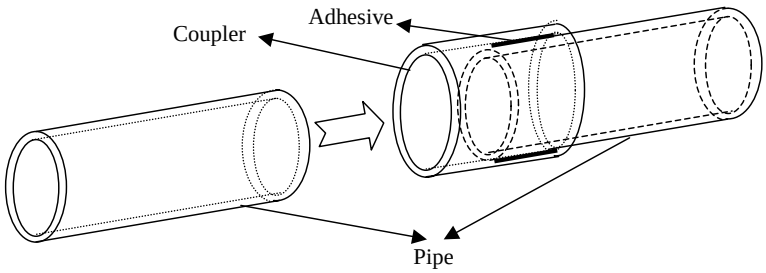

Fig. 1. A common schematic view of pipe joint system.

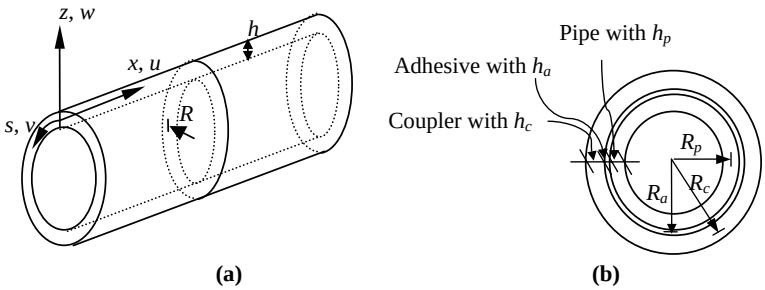

Fig. 2. A schematic geometric view of the pipe joint: (a) common geometric view and (b) cross-section view of joint.

materials with a high electro-mechanic coupling performance as actuators/sensors. In the light of authors' previous work with the smart beam-like joint system (Cheng and Taheri, 2005, 2006), we here can idealize to construct a smart adhesively bonded composite pipe joint system integrated with piezoelectric layers as shown in Fig. 3(b) with comparison to a common coupler as shown in Fig. 3(a). In the developed smart joint system, adjusting the external applied electric fields can induce the relevant deformation of smart laminates, causing the additional force and moment on the joint edge so as to adjust the stress concentration in the joint edge. Obviously, the piezoelectric layers can be freely integrated into any kth layer of a composite coupler. There is no doubt that the stacking sequence of the piezoelectric layers should have a significant effect on the efficiency of such smart joint as well as its size. Therefore, in order to account for the action of the integrated piezoelectric layers, a theoretical model will be established to carry out the peel and shear stresses analysis in the adhesive layer under the application of electro-mechanical loading by using the first-order shear deformation theory (FOST) in the next section.

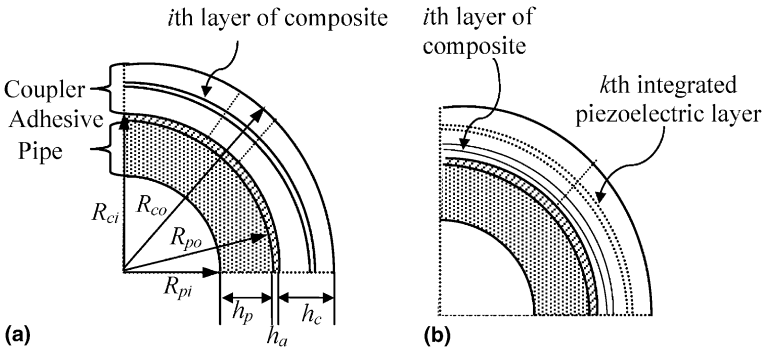

Fig. 3. The basic structures of a common pipe-joint system (a) and the proposed smart pipe joint system integrated with the piezoelectric layer (b).

3. Electro-mechanical theoretical analysis of smart composite pipe joint

In order to theoretically analyze the efficiency of the integrated piezoelectric layers in the developed smart composite pipe joint system as shown in Figs. 1 and 3(b), we employ the first-order shear deformation theory to conduct the detailed stress analysis. The geometric parameters of the smart joint system are as presented in Fig. 4.

Now considering the proposed smart composite pipe joint is subjected to an axial tensile force $\widetilde{N}$, as shown in Fig. 4. Due to the axi-symmetric characteristic of the composite pipe joint system under the axial tensile loading, the overall pipe joint system can be regarded as a two-dimensional problem. Therefore, the displacements u, v and w along the longitudinal, tangential and radial directions for the overlapping pipe section, coupler and bare pipe section can be presented respectively in terms of the first-order shear deformation plate theory as follows:

$$u_i(x,z) = u_{0i}(x) + z\phi_i(x) \tag{1a}$$

$$v_i(x,z) = 0 \tag{1b}$$

$$w_i(x,z) = w(x) \tag{1c}$$

where the subscript 'i' of the above variables denotes the different sections of the composite pipe joint system as shown in Fig. 4. Here, '$i = $ c, p, b' indicate the variables for the connection coupler, overlapping pipe and bare pipe sections, respectively. This definition is also suitable for the future expressions. The u_{0i} and w_i are the mid-plane displacement and ϕ_i is the rotation of the joint different sections.

Furthermore, the strain in the pipes and coupler induced by the above assumed displacement fields in terms of the first-order shear deformation theory as

$$\varepsilon_{1i} = \varepsilon_{xi} = \frac{\partial u_i}{\partial x} = \frac{\partial u_{0i}}{\partial x} + z\frac{\partial \phi_i}{\partial x} \tag{2a}$$

$$\varepsilon_{2i} = \varepsilon_{si} = \frac{w_i}{R_i + z} \tag{2b}$$

$$\varepsilon_{zi} = \frac{\partial w_i}{\partial z} = 0 \tag{2c}$$

$$\varepsilon_{xsi} = \varepsilon_{szi} = 0 \tag{2d}$$

$$\varepsilon_{xzi} = \frac{\partial u_i}{\partial z} + \frac{\partial w_i}{\partial x} = \phi_i + \frac{\partial w_i}{\partial x} \tag{2e}$$

where R_i denotes the radius of the mid-plane for the different sections, for instance, R_p and R_c are the radius of the mid-plane of the pipe wall and coupler wall, respectively, as shown in Fig. 2.

Further, considering the effects of the piezoelectric layer with the poling direction along the z-axis, the stress–strain relationships of the kth lamina in the shell coordinate system are represented by

$$\sigma_{ij}^k = C_{ijkl}^k \varepsilon_{kl} - e_{ijk}^k E_k \tag{3a}$$

$$D_i^k = e_{ikl}^k \varepsilon_{kl} + k_{ij}^k E_j \tag{3b}$$

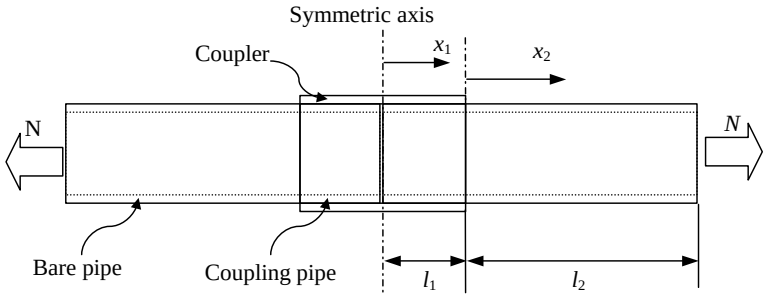

Fig. 4. A schematic view of the different sections of the composite pipe joint system.

where the superscript "k" denotes the kth layer of the laminate panel. C_{ijkl}, e_{ijk} and k_{ij} are the elastic, piezoelectric and dielectric constants for the lamina, respectively. It is noted that the piezoelectric coefficients are equal to zero for the elastic composite layers. Moreover, when the piezoelectric layer is subjected to the externally applied electric field as an actuator, the additional forces/moments can be produced to enhance/reduce the structure deformation. Otherwise, as the piezoelectric layer acts as a sensor, Eq. (3b) can be used to theoretically induce the sensing equation for monitoring the system deformation after the deformation of pipe joint system is determined (Lee and Moon, 1990; Cheng et al., 2005a,b). And in experiment, some workers had successfully applied the embedded piezoelectric sensor to measure the stress in adhesive joint (Anderson et al., 1994).

Most of the reinforcements used for the centrifugal casting are orthotropic, including chopped-strand mats, woven roving, unidirectional fabrics etc. (Yang et al., 2002). Then, considering the strain expression in Eq. (2) and fiber distribution angle of the kth layer, the stress–strain relationships of the composite pipe walls can be further described in the following forms:

$$\begin{Bmatrix} \sigma_1 \\ \sigma_2 \end{Bmatrix}^k = \begin{bmatrix} \overline{Q}_{11} & \overline{Q}_{12} \\ \overline{Q}_{21} & \overline{Q}_{22} \end{bmatrix}^k \begin{Bmatrix} \varepsilon_1 \\ \varepsilon_2 \end{Bmatrix} - \begin{bmatrix} \bar{e}_{31} \\ \bar{e}_{32} \end{bmatrix}^k \{E_3\}^k \tag{4a}$$

$$\{\sigma_5\}^k = [k\overline{Q}_{55}]^k \{\varepsilon_5\} \tag{4b}$$

where $\overline{Q}_{ij}$ are the transformed stiffness and can be obtained from the relative lamina.

For a general cross-ply laminate, the resultant forces and moments can be obtained by integration of the stresses as shown in Eq. (4). Integration through the thickness cross section of each component of the smart pipe joint system yields the following resultant forces and moments (Ugural, 1999):

$$\begin{aligned} N_{xi} &= \int_{-\frac{h}{2}}^{\frac{h}{2}} \frac{R_i + z}{R_i} \sigma_{1i}\,\mathrm{d}z = \sum_{k=1}^{n} \int_{h_k}^{h_{k+1}} \frac{R_i + z}{R_i} \left(\overline{Q}_{11i}^k \varepsilon_{1i} + \overline{Q}_{12i}^k \varepsilon_{2i} - \bar{e}_{31}^k E_3^k\right) \mathrm{d}z \\ &= \sum_{k=1}^{n} \int_{h_k}^{h_{k+1}} \frac{R_i + z}{R_i} \left[\overline{Q}_{11i}^k \left(\frac{\partial u_{0i}}{\partial x} + z\frac{\partial \phi_i}{\partial x}\right) + \overline{Q}_{12i}^k \frac{w_i}{R_i + z} - \bar{e}_{31}^k E_3^k\right] \mathrm{d}z \\ &= A_{i11}\frac{\partial u_{0i}}{\partial x} + B_{i11}\frac{\partial \phi_i}{\partial x} + E_{i12} w_i - N_{xc}^{\mathrm{PZT}} \end{aligned} \tag{5a}$$

$$\begin{aligned} M_{xi} &= \int_{-\frac{h}{2}}^{\frac{h}{2}} \frac{R_i + z}{R_i} z\sigma_{1i}\,\mathrm{d}z = \sum_{k=1}^{n} \int_{h_k}^{h_{k+1}} \frac{R_i + z}{R_i} \left(\overline{Q}_{11i}^k \varepsilon_1 + \overline{Q}_{12i}^k \varepsilon_2 - \bar{e}_{31}^k E_3^k\right) z\,\mathrm{d}z \\ &= \sum_{k=1}^{n} \int_{h_k}^{h_{k+1}} \frac{R_i + z}{R_i} \left[\overline{Q}_{11i}^k \left(\frac{\partial u_{0i}}{\partial x} + z\frac{\partial \phi_i}{\partial x}\right) + \overline{Q}_{12i}^k \frac{w_i}{R_i + z} - \bar{e}_{31}^k E_3^k\right] z\,\mathrm{d}z \\ &= B_{i11}\frac{\partial u_{0i}}{\partial x} + D_{i11}\frac{\partial \phi_i}{\partial x} + F_{i12} w_i - M_{xc}^{\mathrm{PZT}} \end{aligned} \tag{5b}$$

$$\begin{aligned} N_{si} &= \int_{-\frac{h}{2}}^{\frac{h}{2}} \frac{R_i + z}{R_i} \sigma_{2i}\,\mathrm{d}z = \sum_{k=1}^{n} \int_{h_k}^{h_{k+1}} \frac{R_i + z}{R_i} \left(\overline{Q}_{21i}^k \varepsilon_1 + \overline{Q}_{22i}^k \varepsilon_2 - \bar{e}_{32}^k E_3^k\right) \mathrm{d}z \\ &= \sum_{k=1}^{n} \int_{h_k}^{h_{k+1}} \frac{R_i + z}{R_i} \left[\overline{Q}_{21i}^k \left(\frac{\partial u_{0i}}{\partial x} + z\frac{\partial \phi_i}{\partial x}\right) + \overline{Q}_{22i}^k \frac{w_i}{R_i + z} - \bar{e}_{32}^k E_3^k\right] \mathrm{d}z \\ &= A_{i21}\frac{\partial u_{0i}}{\partial x} + B_{i21}\frac{\partial \phi_i}{\partial x} + E_{22i} w_i - N_{sc}^{\mathrm{PZT}} \end{aligned} \tag{5c}$$

$$\begin{aligned} Q_{xi} &= \int_{-\frac{h}{2}}^{\frac{h}{2}} \sigma_5\,\mathrm{d}z = \sum_{k=1}^{n} \int_{h_k}^{h_{k+1}} K\overline{Q}_{55i}^k \varepsilon_{xz}\,\mathrm{d}z \\ &= \sum_{k=1}^{n} \int_{h_k}^{h_{k+1}} K\overline{Q}_{55i}^k \left(\phi_i + \frac{\partial w_i}{\partial x}\right) \mathrm{d}z \\ &= A_{i55}\phi_i + A_{i55}\frac{\partial w_i}{\partial x} \end{aligned} \tag{5d}$$

where A_{ij}, B_{ij}, D_{ij}, E_{ij} and F_{ij} are defined as the stiffness matrix for the convenience of future equation derivation. Here, the resultant forces and moments induced by the piezoelectric layer as actuators can be presented in the following forms:

$$N_{xc}^{\mathrm{PZT}} = \sum_{k=1}^{n} \int_{h_k}^{h_{k+1}} \frac{R_i + z}{R_i} \bar{e}_{31}^{k} E_3^k \, \mathrm{d}z \tag{6a}$$

$$M_{xc}^{\mathrm{PZT}} = \sum_{k=1}^{n} \int_{h_k}^{h_{k+1}} \frac{R_i + z}{R_i} z \bar{e}_{31}^{k} E_3^k \, \mathrm{d}z \tag{6b}$$

$$N_{sc}^{\mathrm{PZT}} = \sum_{k=1}^{n} \int_{h_k}^{h_{k+1}} \frac{R_i + z}{R_i} \bar{e}_{32}^{k} E_3^k \, \mathrm{d}z \tag{6c}$$

It is evident that the electric field-induced additional forces and moments can be controlled through adjusting the lamina thickness and applied electric field in the different piezoelectric layers. It is further noted that in order to consider the effect of the surface covered electrode region $[x_0, x_1]$ in the piezoelectric layers, we can apply the Heaviside step function to describe the applied electric field in the following form:

$$E_3^k = -\frac{V^k}{h^k}[H(x - x_0) - H(x - x_1)] \tag{6d}$$

with $H(x - x_a)$ being the Heaviside step function.

Now considering the infinitesimal elements of the joint section and using the static equilibrium conditions for each layer as shown in Fig. 5, we can obtain the fundamental equilibrium equations for any segment of the smart composite pipe joint system as follows:

In the connection coupler, we have

$$\frac{\partial N_{xc}}{\partial x} = -\frac{R_{\mathrm{ci}}}{R_{\mathrm{c}}}\tau \tag{7a}$$

$$\frac{\partial M_{xc}}{\partial x} - Q_{xc} = \frac{h_{\mathrm{c}}}{2}\frac{R_{\mathrm{ci}}}{R_{\mathrm{c}}}\tau \tag{7b}$$

$$\frac{\partial Q_{xc}}{\partial x} - \frac{N_{sc}}{R_{\mathrm{c}}} = \frac{R_{\mathrm{ci}}}{R_{\mathrm{c}}} q \tag{7c}$$

and in the overlapping pipe section as shown in Figs. 4 and 5, we can present the equilibrium equations as

$$\frac{\partial N_{xp}}{\partial x} = \frac{R_{\mathrm{po}}}{R_{\mathrm{p}}}\tau \tag{8a}$$

$$\frac{\partial M_{xp}}{\partial x} - Q_{xp} = \frac{h_{\mathrm{p}}}{2}\frac{R_{\mathrm{po}}}{R_{\mathrm{p}}}\tau \tag{8b}$$

$$\frac{\partial Q_{xp}}{\partial x} - \frac{N_{sp}}{R_{\mathrm{p}}} = -\frac{R_{\mathrm{po}}}{R_{\mathrm{p}}} q \tag{8c}$$

where R_{c} and R_{p} are the central radius of the coupler and pipe, respectively. And, R_{po} is the outer radius of the pipe and R_{ci} the inner radius of the coupler.

Here τ and q are the shear stress and peel stress in the adhesive layer caused by the inhomogeneity of the longitudinal, tangential and radial deformations in the pipe and coupler. The shear stress τ in the adhesive layer can be expressed by the longitudinal displacement change from the inner surface of the coupler to the outer surface of pipe and the relative first-order axial derivative of their radial deflections in the following form:

$$\tau = \frac{G_{\mathrm{a}}}{h_{\mathrm{a}}}\left[(u_{0\mathrm{p}} - u_{0\mathrm{c}}) + \left(\frac{h_{\mathrm{p}}}{2}\phi_{\mathrm{p}} + \frac{h_{\mathrm{c}}}{2}\phi_{\mathrm{c}}\right)\right] - \frac{G_{\mathrm{a}}}{2}\left(\frac{\partial w_{\mathrm{p}}}{\partial x} + \frac{\partial w_{\mathrm{c}}}{\partial x}\right) \tag{9}$$

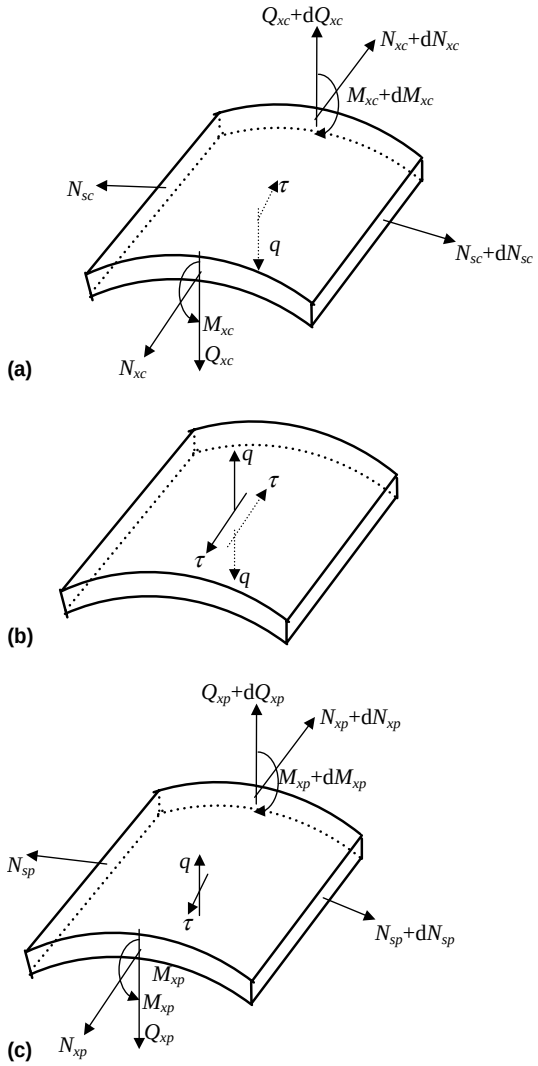

Fig. 5. The stress and forces on the infinitesimal substructures of a joint system: (a) the top layer (connection coupler), (b) the adhesive layer, (c) the bottom layer (main pipe).

The peel stress q is mainly caused by the radial displacements difference between the coupler and pipe and written as

$$q = \frac{E_a}{h_a}(w_c - w_p) \tag{10}$$

where G_a and E_a are the shear and Young's modulus of the adhesive layer with the thickness h_a.

Similarly, the conditions of force equilibrium for the bare pipe section, as shown in Fig. 4, can be obtained by neglecting the shear and peel effects from Eq. (10) as follows:

$$\frac{\partial N_{xp}}{\partial x} = 0 \tag{11a}$$

$$\frac{\partial M_{xp}}{\partial x} - Q_{xp} = 0 \tag{11b}$$

$$\frac{\partial Q_{xp}}{\partial x} - \frac{N_{sp}}{R_p} = 0 \tag{11c}$$

Furthermore, the relevant boundary conditions and continuity conditions between the different sections of the smart composite pipe joint system can be presented in the following details when the axi-symmetric tension loading is applied to the pipe end as shown in Fig. 4:

At $x_1 = 0$, due to the free overlapping pipe and the symmetric characteristics of the joint system for the coupler, we have the relevant boundary conditions for the overlapping pipe and coupler respectively as

$$N_{xp}(0) = 0, \qquad M_{sp}(0) = 0, \qquad Q_{xp}(0) = 0 \tag{12a}$$

$$u_{0c}(0) = 0, \qquad \frac{dw_c}{dx}(0) = 0, \qquad Q_{xc}(0) = 0 \tag{12b}$$

Similarly, at $x_1 = l_1$ due to the free edge of the smart coupler end, we have

$$N_{xc}(l_1) = 0, \qquad M_{sc}(l_1) = 0, \qquad Q_{xc}(l_1) = 0 \tag{12c}$$

While at $x_1 = l_1$ and $x_2 = 0$, the overlapping pipe section and the bare pipe section is continuous, we can present the continuity conditions for the pipe as

$$\begin{aligned} &u_{0p}(l_1) = u_{0b}(0), \qquad \phi_p(l_1) = \phi_b(0), \qquad w_p(l_1) = w_b(0) \\ &\frac{du_{0p}}{dx}(l_1) = \frac{du_{0b}}{dx}(0), \qquad \frac{d\phi_p}{dx}(l_1) = \frac{d\phi_b}{dx}(0), \qquad \frac{dw_p}{dx}(l_1) = \frac{dw_b}{dx}(0) \end{aligned} \tag{12d}$$

Finally, at $x_2 = l_2$, i.e. the end of the joint pipe, it is subjected to a tensile loading, which can yield

$$N_{xb}(l_2) = \widetilde{N}_{x0}, \qquad M_{sb}(l_2) = 0, \qquad Q_{xb}(l_2) = 0 \tag{12e}$$

Now, substituting the relevant resultant forces and moments into the above force equilibrium equations in Eqs. (7), (8) and (11), we can obtain the displacement-based governing differential equations for the smart composite pipe joint system in the following forms:

In the coupler, we have

$$\begin{aligned} &A_{c11}\frac{\partial^2 u_{0c}}{\partial x^2} + B_{c11}\frac{\partial^2 \phi_c}{\partial x^2} + E_{c12}\frac{\partial w_c}{\partial x} \\ &\quad = -\frac{R_{ci}}{R_c}\left\{\frac{G_a}{h_a}\left[(u_{p0} - u_{c0}) + \left(\frac{h_p}{2}\phi_p + \frac{h_c}{2}\phi_c\right)\right] - \frac{G_a}{2}\left(\frac{\partial w_p}{\partial x} + \frac{\partial w_c}{\partial x}\right)\right\} + \frac{\partial N_{xc}^{PZT}}{\partial x} \end{aligned} \tag{13a}$$

$$\begin{aligned} &B_{c11}\frac{\partial^2 u_{0c}}{\partial x^2} + D_{c11}\frac{\partial^2 \phi_c}{\partial x^2} + F_{c12}\frac{\partial w_c}{\partial x} - \left(A_{c55}\phi_c + A_{c55}\frac{\partial w_c}{\partial x}\right) \\ &\quad = \frac{h_c}{2}\frac{R_{ci}}{R_c}\left\{\frac{G_a}{h_a}\left[(u_{p0} - u_{c0}) + \left(\frac{h_p}{2}\phi_p + \frac{h_c}{2}\phi_c\right)\right] - \frac{G_a}{2}\left(\frac{\partial w_p}{\partial x} + \frac{\partial w_c}{\partial x}\right)\right\} + \frac{\partial M_{sc}^{PZT}}{\partial x} \end{aligned} \tag{13b}$$

$$A_{c55}\frac{\partial \phi_c}{\partial x} + A_{c55}\frac{\partial^2 w_c}{\partial x^2} - \frac{1}{R_c}\left(A_{c21}\frac{\partial u_{0c}}{\partial x} + B_{c21}\frac{\partial \phi_c}{\partial x} + E_{c22}w_c\right) = \frac{R_{ci}}{R_c}\frac{E_a}{h_a}(w_c - w_p) - \frac{N_{sc}^{PZT}}{R_c} \tag{13c}$$

and the new displacement-based expression for the overlapping pipe section can be rewritten as

$$A_{p11}\frac{\partial^2 u_{0p}}{\partial x^2} + B_{p11}\frac{\partial^2 \phi_p}{\partial x^2} + E_{p12}\frac{\partial w_p}{\partial x} = \frac{R_{po}}{R_p}\left\{\frac{G_a}{h_a}\left[(u_{p0} - u_{c0}) + \left(\frac{h_p}{2}\phi_p + \frac{h_c}{2}\phi_c\right)\right] - \frac{G_a}{2}\left(\frac{\partial w_p}{\partial x} + \frac{\partial w_c}{\partial x}\right)\right\} \tag{14a}$$

$$\begin{aligned} &B_{p11}\frac{\partial^2 u_{0p}}{\partial x^2} + D_{p11}\frac{\partial^2 \phi_p}{\partial x^2} + F_{p12}\frac{\partial w_p}{\partial x} - \left(A_{p55}\phi_p + A_{p55}\frac{\partial w_p}{\partial x}\right) \\ &\quad = \frac{h_p}{2}\frac{R_{po}}{R_p}\left\{\frac{G_a}{h_a}\left[(u_{p0} - u_{c0}) + \left(\frac{h_p}{2}\phi_p + \frac{h_c}{2}\phi_c\right)\right] - \frac{G_a}{2}\left(\frac{\partial w_p}{\partial x} + \frac{\partial w_c}{\partial x}\right)\right\} \end{aligned} \tag{14b}$$

$$A_{p55}\frac{\partial \phi_p}{\partial x} + A_{p55}\frac{\partial^2 w_p}{\partial x^2} - \frac{1}{R_p}\left(A_{p21}\frac{\partial u_{0p}}{\partial x} + B_{p21}\frac{\partial \phi_p}{\partial x} + E_{p22}w_p\right) = -\frac{R_{po}}{R_p}\frac{E_a}{h_a}(w_c - w_p) \tag{14c}$$

Similarly, we can present the displacement-based governing equations for the bare pipe section as

$$A_{p11}\frac{\partial^2 u_{0p}}{\partial x^2}+B_{p11}\frac{\partial^2 \phi_p}{\partial x^2}+E_{p12}\frac{\partial w_p}{\partial x}=0 \tag{15a}$$

$$B_{p11}\frac{\partial^2 u_{0p}}{\partial x^2}+D_{p11}\frac{\partial^2 \phi_p}{\partial x^2}+F_{p12}\frac{\partial w_p}{\partial x}-\left(A_{p55}\phi_p+A_{p55}\frac{\partial w_p}{\partial x}\right)=0 \tag{15b}$$

$$A_{p55}\frac{\partial \phi_p}{\partial x}+A_{p55}\frac{\partial^2 w_p}{\partial x^2}-\frac{1}{R_p}\left(A_{p21}\frac{\partial u_{0p}}{\partial x}+B_{p21}\frac{\partial \phi_p}{\partial x}+E_{p22}w_p\right)=0 \tag{15c}$$

Obviously, the above displacement-based governing equations for the different sections are second-order differential equations with the boundary-value conditions and continuity conditions. Here, we can apply the state-space method to conveniently solve the above differential equations. In order to produce the state equations, we have to introduce some unknown variables to simplify the above equations as follows:

$$Z_1=u_{0c},\quad Z_2=Z_1'=\frac{\partial u_{0c}}{\partial x},\quad Z_3=\phi_c,\quad Z_4=Z_3'=\frac{\partial \phi_c}{\partial x},\quad Z_5=w_c,\quad Z_6=Z_5'=\frac{\partial w_c}{\partial x}$$

$$Z_7=u_{0p},\quad Z_8=Z_7'=\frac{\partial u_{0p}}{\partial x},\quad Z_9=\phi_p,\quad Z_{10}=Z_9'=\frac{\partial \phi_p}{\partial x},\quad Z_{11}=w_p,\quad Z_{12}=Z_{11}'=\frac{\partial w_p}{\partial x}$$

$$X_1=u_{0b},\quad X_2=X_1'=\frac{\partial u_{0b}}{\partial x},\quad X_3=\phi_b,\quad X_4=X_3'=\frac{\partial \phi_b}{\partial x},\quad X_5=w_b,\quad X_6=X_5'=\frac{\partial w_b}{\partial x}$$

Using the above unknown variables, the displacement-based governing Eqs. (13)-(15) can be represented by the first-order state equation systems respectively in the following matrix forms:

$$\{Z\}'=[A]\{Z\}+[\Lambda] \tag{16}$$

$$\{X\}'=[B]\{X\} \tag{17}$$

and clearly in terms of Eqs. (9) and (10), the peel and shear stresses in the adhesive layer of the smart composite pipe joint system can be obtained from

$$q=\left[0\quad 0\quad 0\quad 0\quad \frac{E_a}{h_a}\quad 0\quad 0\quad 0\quad 0\quad 0\quad -\frac{E_a}{h_a}\quad 0\right]\{Z\} \tag{18a}$$

$$\tau=\left[-\frac{G_a}{h_a}\quad 0\quad \frac{G_a h_c}{2h_a}\quad 0\quad 0\quad -\frac{G_a}{2}\quad \frac{G_a}{h_a}\quad 0\quad \frac{G_a h_p}{2h_a}\quad 0\quad 0\quad 0\right]\{Z\} \tag{18b}$$

where the detailed non-zero components of matrix $[A]$ and $[B]$ are shown in the appendix. Here, $[\Lambda]$ is a 12×1 dimensions matrix and has the following non-zero components:

$$\Lambda(2,1)=\frac{D_{c11}N_{xc}^{P'}-B_{c11}M_{xc}^{P'}}{A_{c11}D_{c11}-B_{c11}^2},\quad \Lambda(4,1)=\frac{A_{c11}M_{xc}^{P'}-B_{c11}N_{xc}^{P'}}{A_{c11}D_{c11}-B_{c11}^2}\quad \text{and}\quad \Lambda(6,1)=-\frac{N_{sc}^{PZT}}{A_{c55}R_c}$$

with the following definitions:

$$N_{xc}^{P'}=N_{xc}^{PZT}[\delta(x-l)-\delta(x+l)],\qquad M_{xc}^{P'}=M_{xc}^{PZT}[\delta(x-l)-\delta(x+l)]$$

The common exponent analytical solutions for the above two state Eqs. (16) and (17) can be generally expressed in the following forms:

$$Z(x)=e^{x[H]}\{k_1\}+e^{x[H]}\int^x e^{-\vartheta[H]}[\Lambda]\,d\vartheta \tag{19}$$

$$X(x)=e^{x[\Lambda]}\{k_2\} \tag{20}$$

where $\{k_1\}$ is a vector with 12 unknown coefficients determined by the relevant boundary and continuity conditions at $x=0$, l_1 and $\{k_2\}$ is a vector with six unknown coefficients calculated by the boundary and continuity conditions at $x=0,l_2$, as given in Eq. (11), with the help of strain–stress and strain–displacement relationships (Eqs. (2) and (3)). After the unknown coefficients $\{k_i\}$ $(i=1,2)$ are determined by the boundary

and continuity conditions, the peel and shear stresses' distribution in the adhesive layer of the developed smart composite pipe joint system can be analytically calculated by Eq. (18).

4. Numerical analysis and discussion

In terms of the theoretical analysis model of the stress distribution for the smart composite pipe joint system in the above section, we here will present some detailed numerical examples to validate the integrity of developed joint system with the integrated piezoelectric layers in the coupler. Here, we will take the 54-degree filament-wound E-glass/Derakane 470 composite pipe as the calculation samples for the pipe and the coupler. The following material properties and geometric parameters of the composite pipe and coupler, adhesive and piezoelectric ceramics are used in present simulations as

Composite layer: $E_1 = 25.2$ GPa, $E_2 = 7.5$ GPa, $E_{12} = 2.4$ GPa, $v_{12} = 0.32$.
Epoxy adhesive: $E_a = 0.96$ GPa, $G_a = 0.34$ GPa, $\mu_3 = 0.412$.
Piezoelectric materials: $E_{PZT} = 8.4 \times 10^{10}$ N/m^2, $\mu_3 = 0.22$, $d_{31} = d_{32} = -310 \times 10^{-12}$ m/V.
Geometric parameters: $l_1 = 25.4$ mm, $l_2 = 127$ mm, $h_a = 0.0127$ mm, $h_p = h_c = 2.54$ mm, $R_{pi} = 50.8$ mm.

Now, considering the developed smart composite pipe with the above materials properties and global geometries subjected to 25 kN axial load, we used the first-order shear deformation-based theoretical model developed in the last section to calculate the detailed numerical examples for confirming the action and efficiency of the integrated piezoelectric layers. Firstly, we assumed that the developed smart coupler was laminated by the following stacking sequence [Comp/PZT1/Comp/Comp/PZT2/Comp] with the relative thicknesses $\left[\frac{h_c}{6}/\frac{h_c}{6}/\frac{h_c}{6}/\frac{h_c}{6}/\frac{h_c}{6}/\frac{h_c}{6}\right]$, where the piezoelectric layers PZT1 and PZT2 were subjected to the electric fields E_3^1 and E_3^2, respectively. Then, some detailed calculations of the peel and shear stresses distribution for such stacking sequence and lamina geometries of the joint under the combined mechanical axial loading and the applied electric fields $E_3^1 = E_3^2$, which is set as study Case 1, were firstly carried out. The results for Case 1 are shown in Fig. 6 for the peel stress distribution and Fig. 7 for the shear stress distribution. The numerical results in Figs. 6 and 7 both indicate that the peel/shear stress concentrations always present in the end edge region of the joint and can be significantly and adaptively controlled by the electric fields applied to the integrated piezoelectric layers. Further, Fig. 8 presents the detailed influences of the different applied electric fields applied to the different piezoelectric layers on the maximum peel/shear stresses for Case 1, i.e. $E_3^1 = E_3^2$, which result in $N_i^{PZT} \neq 0$ and $M_i^{PZT} \approx 0$, and, Case 2, i.e. $E_3^2 = -E_3^1$ which can lead to $N_i^{PZT} \approx 0$ and $M_i^{PZT} \neq 0$. From the results in Fig. 8, it is seen that the applied negative electric field E_3^1 can dominantly reduce both the maximum peel and shear stresses but the positive electric field E_3^1 increases the maximum peel and shear stresses in Case 1. In Case 2, the enhancement actions of the integrated piezoelectric layers become more complicated as

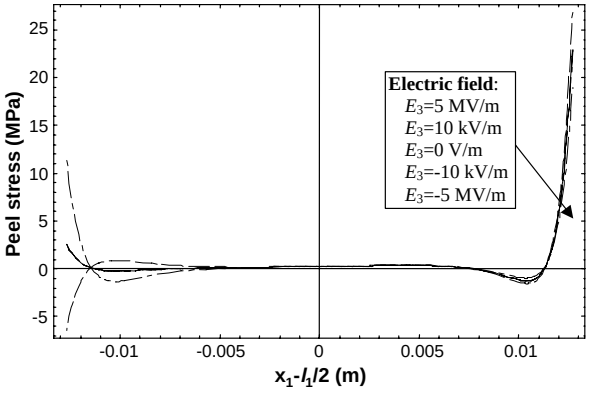

Fig. 6. The influence of the applied electric fields in the integrated piezoelectric layers on the peel stress distribution in the adhesive layer for Case 1.

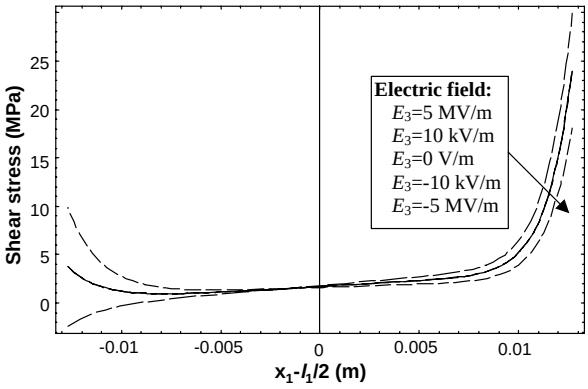

Fig. 7. The effect of the applied electric fields in the integrated piezoelectric layers on the shear stress distribution in the adhesive layer for Case 1.

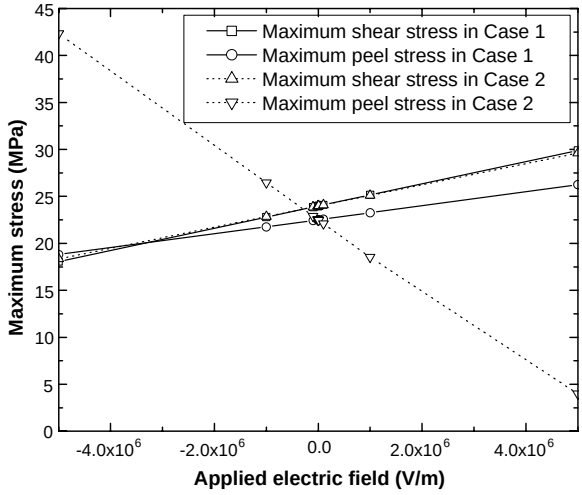

Fig. 8. The influence of the applied electric fields on the maximum peel and shear stress in the adhesive layer for Cases 1 and 2.

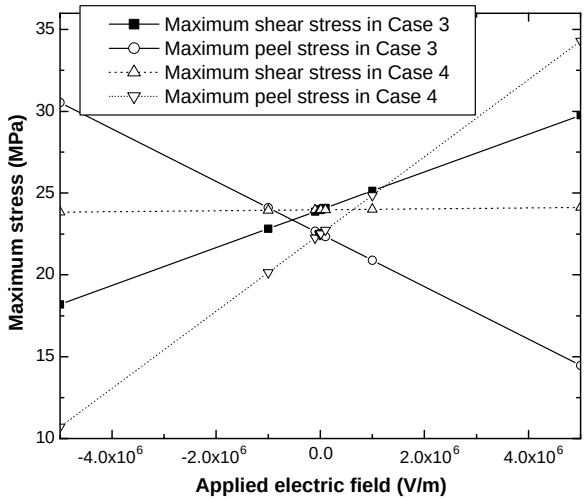

Fig. 9. The comparison of the effect of applied electric fields on the maximum peel and shear stress in the adhesive layer for Cases 3 and 4.

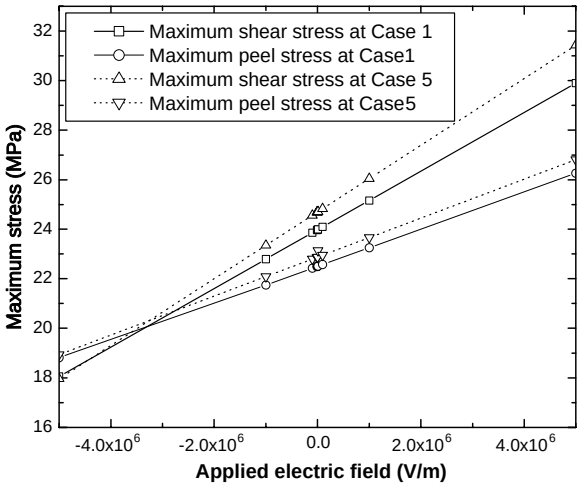

Fig. 10. The comparison of the maximum peel/shear for the smart composite pipe joint systems by the integrated piezoelectric layer with the different thickness.

shown in Fig. 8, namely, the applied negative electric field E_3^1 can decrease the maximum shear stress but remarkably increase the maximum peel stress; by contrast, a positive applied electric field can achieve the opposite effect. Furthermore, two other study cases for such composite pipe joint, involving the study Case 3: $E_3^1 \neq 0$ and $E_3^2 = 0$, and study Case 4: $E_3^1 = 0$ and $E_3^2 \neq 0$, which both result in $N_i^{\mathrm{PZT}} \neq 0$ and $M_i^{\mathrm{PZT}} \neq 0$, were modeled and studied as depicted in Fig. 9. In Case 3, it is obvious from Fig. 9 that an applied negative electric field E_3^1 can notably reduce the maximum shear stress. However, the positive electric fields increase the maximum shear stress. The effects of applied electric fields on the maximum peel stress are to the opposite of the maximum shear stress. With Comparison to the results of Case 3, the applied electric fields in Case 4 only have little influence on the maximum shear stress in the adhesive layer. However, the negative electric fields can evidently reduce the maximum peel stress, as presented in Fig. 9.

We further considered the thickness effect of the integrated piezoelectric layers on the enhancement/reduction efficiency of maximum peel and shear stress. Here, the smart coupler with the lamina thickness parameters $\left[\frac{h_c}{6} / \frac{h_c}{4} / \frac{h_c}{12} / \frac{h_c}{12} / \frac{h_c}{4} / \frac{h_c}{6}\right]$ was utilized to compute and analyze the detailed size effect. Under the same axial tensile loading, we calculated the numerical results of such smart composite pipe joint system for these relative study

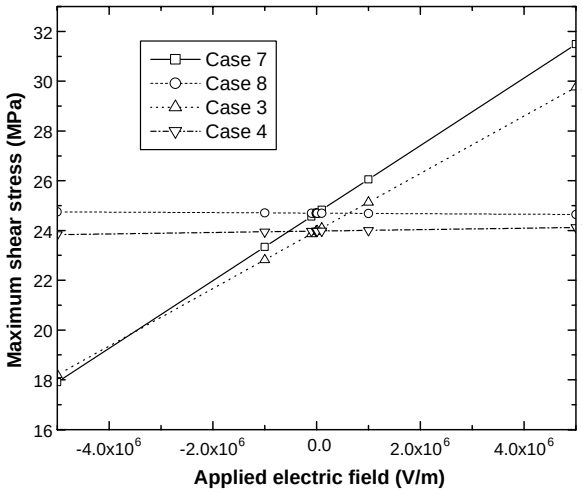

Fig. 11. The comparison of the effect of applied electric field on the maximum shear stress for Cases 3, 4, 7 and 8.

cases: Case 5: $E_3^1 = E_3^2$, Case 6: $E_3^2 = -E_3^1$, Case 7: $E_3^1 \neq 0$ and $E_3^2 = 0$ and Case 8: $E_3^1 = 0$ and $E_3^2 \neq 0$. Fig. 10 displays the numerical comparison of the maximum peel/shear stresses between the study Case 1 and Case 5, which indicates that the thickness of laminated piezoelectric layers can change the maximum distribution stress. And some more detailed comparisons for the size effect of the maximum peel/shear stresses among the different study cases were further presented in Figs. 11–13, which also revealed and confirmed the influence of the integrated piezoelectric layers thickness on the maximum peel/shear stresses. From the numerical comparisons, it is clear that the thickness of the integrated piezoelectric layers have a significant effect on the maximum peel and shear stress, and thicker integrated piezoelectric layers can enhance the enhancement/reduction of the maximum peel/shear stress under the relevant applied electric fields. But due to the change of the coupler overall material properties caused by thickening the integrated piezoelectric layers, the initial maximum peel/shear stresses (i.e. the maximum peel/shear stresses at $E_3^1 = E_3^2 = 0$) also have a slight increase, as shown in Figs. 10–13, which further clarifies the integrity of the developed strength improvement method and designablity of the composite pipe joint.

In a word, from the above detailed numerical analyses, it is clear that integrated piezoelectric layers can significantly reduce the maximum peel/shear stress in the adhesive layer with a suitable choice of stacking

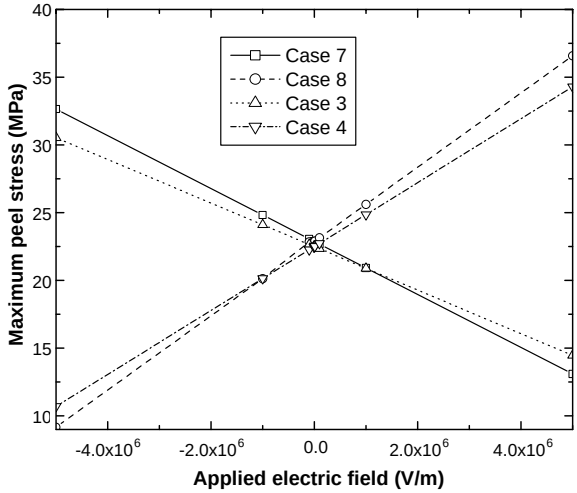

Fig. 12. The comparison of the effect of applied electric field on the maximum peel stress for Cases 3, 4, 7 and 8.

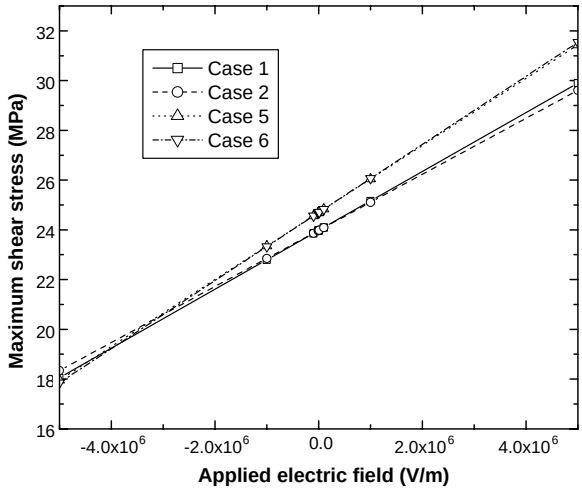

Fig. 13. The comparison of the effect of applied electric field on the maximum shear stress for Cases 1, 2, 5 and 6.

sequence, lamina thickness and applied electric fields so as to adaptively enhance the failure strength of such composite pipe joint. Of course, the integrated piezoelectric layers can also be used as sensors to monitor the joint structural deformation. The sensing results can be obtained from sensing equation as shown in Eq. (3b) after the structural deformation determined. Here, we neglected the detailed theoretical work on the sensing functions of the integrated piezoelectric layers.

5. Conclusion

Due to the high performance electro-mechanical coupling of piezoelectric materials, a smart adhesively bonded composite pipe joint system was proposed to adaptively reduce the stress concentration effect in the adhesive layer via the coupler integrated with piezoelectric layers as sensor/actuator. In order to analyze the efficiency of the integrated piezoelectric layers, an electro-mechanical theoretical analysis model based on first-order shear deformation theory was established to develop the fundamental equations for the analyses of the developed smart composite pipe joint system when subjected to an axial tensile loading and electric fields. Further, the state-space method was utilized to deduce the final analytical solutions, including the peel and shear stress in the adhesive layer. Finally, some detailed numerical examples were presented to compare the action and efficiency of the integrated piezoelectric layers with different lamina thicknesses and applied electric fields, which confirmed the integrity of developed smart adhesive composite pipe joint system. The numerical results also validated that the peel/shear stress distribution can be optimized by choosing the suitable piezoelectric materials, the geometries and applied electric fields to adaptively reduce the peel/shear stress concentration.

Appendix A

The non-zero components of the matrices $[A]$ and $[B]$ are presented as follows:

$$A[1,2]=A[3,4]=A[5,6]=A[7,8]=A[9,10]=A[11,12]=1$$

$$A[2,1]=\frac{\frac{D_{c11}R_{ci}G_a}{R_ch_a}+\frac{h_cB_{c11}R_{ci}G_a}{2R_ch_a}}{A_{c11}D_{c11}-B_{c11}^2},\qquad A[2,3]=\frac{-D_{c11}\frac{h_cR_{ci}G_a}{2R_ch_a}-B_{c11}\left(A_{c55}+\frac{h_c^2R_{ci}G_a}{4R_ch_a}\right)}{A_{c11}D_{c11}-B_{c11}^2}$$

$$A[2,6]=\frac{D_{c11}\left(\frac{R_{ci}G_a}{2R_c}-E_{c12}\right)-B_{c11}\left(A_{c55}-\frac{h_cR_{ci}G_a}{4R_c}-F_{c12}\right)}{A_{c11}D_{c11}-B_{c11}^2},\qquad A[2,7]=\frac{-D_{c11}\frac{R_{ci}G_a}{R_ch_a}-B_{c11}\frac{h_cR_{ci}G_a}{2R_ch_a}}{A_{c11}D_{c11}-B_{c11}^2}$$

$$A[2,9]=\frac{-D_{c11}\frac{h_pR_{ci}G_a}{2R_ch_a}-B_{c11}\frac{h_ch_pR_{ci}G_a}{4R_ch_a}}{A_{c11}D_{c11}-B_{c11}^2},\qquad A[2,12]=\frac{D_{c11}\frac{R_{ci}G_a}{2R_c}+B_{c11}\frac{h_cR_{ci}G_a}{4R_c}}{A_{c11}D_{c11}-B_{c11}^2}$$

$$A[4,1]=\frac{-A_{c11}\frac{h_cR_{ci}G_a}{2R_ch_a}-B_{c11}\frac{R_{ci}G_a}{R_ch_a}}{A_{c11}D_{c11}-B_{c11}^2},\qquad A[4,3]=\frac{A_{c11}\left(A_{c55}+\frac{h_c^2R_{ci}G_a}{4R_ch_a}\right)+B_{c11}\frac{h_cR_{ci}G_a}{2R_ch_a}}{A_{c11}D_{c11}-B_{c11}^2}$$

$$A[4,6]=\frac{A_{c11}\left(A_{c55}-\frac{h_cR_{ci}G_a}{4R_c}-F_{c12}\right)-B_{c11}\left(\frac{R_{ci}G_a}{2R_c}-E_{c12}\right)}{A_{c11}D_{c11}-B_{c11}^2},\qquad A[4,7]=\frac{A_{c11}\frac{h_cR_{ci}G_a}{2R_ch_a}+B_{c11}\frac{R_{ci}G_a}{R_ch_a}}{A_{c11}D_{c11}-B_{c11}^2}$$

$$A[4,9]=\frac{A_{c11}\frac{h_ch_pR_{ci}G_a}{4R_ch_a}+B_{c11}\frac{h_pR_{ci}G_a}{2R_ch_a}}{A_{c11}D_{c11}-B_{c11}^2},\qquad A[4,12]=\frac{-A_{c11}\frac{h_cR_{ci}G_a}{4R_c}-B_{c11}\frac{R_{ci}G_a}{2R_c}}{A_{c11}D_{c11}-B_{c11}^2}$$

$$A[6,2]=\frac{A_{c21}}{R_cA_{c55}},\qquad A[6,4]=\frac{1}{A_{c55}}\left(\frac{B_{c21}}{R_c}-A_{c55}\right),\qquad A[6,5]=\frac{1}{A_{c55}}\left(\frac{E_{c22}}{R_c}+\frac{R_{ci}}{R_c}\frac{E_a}{h_a}\right)$$

$$A[6,11]=-\frac{1}{A_{c55}}\frac{R_{ci}}{R_c}\frac{E_a}{h_a}$$

$$A[8,1]=\frac{-D_{p11}\frac{R_{po}G_a}{R_ph_a}+B_{p11}\frac{h_pR_{po}G_a}{2R_ph_a}}{A_{p11}D_{p11}-B_{p11}^2},\qquad A[8,3]=\frac{D_{p11}\frac{h_cR_{po}G_a}{2R_ph_a}-B_{p11}\frac{h_ch_pR_{po}G_a}{4R_ph_a}}{A_{p11}D_{p11}-B_{p11}^2}$$

$$A[8,6]=\frac{-D_{p11}\frac{R_{po}G_a}{2R_p}+B_{p11}\frac{h_pR_{po}G_a}{4R_p}}{A_{p11}D_{p11}-B_{p11}^2},\qquad A[8,7]=\frac{D_{p11}\frac{R_{po}G_a}{R_ph_a}-B_{p11}\frac{h_pR_{po}G_a}{2R_ph_a}}{A_{p11}D_{p11}-B_{p11}^2}$$

$$A[8,9]=\frac{D_{p11}\frac{h_pR_{po}G_a}{2R_ph_a}-B_{p11}\left(A_{p55}+\frac{h_p^2R_{po}G_a}{4R_ph_a}\right)}{A_{p11}D_{p11}-B_{p11}^2}$$

$$A[8,12]=\frac{-D_{p11}\left(E_{p12}+\frac{R_{po}G_a}{2R_p}\right)-B_{p11}\left(A_{p55}-F_{p12}-\frac{h_pR_{po}G_a}{4R_p}\right)}{A_{p11}D_{p11}-B_{p11}^2}$$

$$A[10,1]=\frac{-A_{p11}\frac{h_pR_{po}G_a}{2R_ph_a}+B_{p11}\frac{R_{po}G_a}{R_ph_a}}{A_{p11}D_{p11}-B_{p11}^2},\qquad A[10,3]=\frac{A_{p11}\frac{h_ch_pR_{po}G_a}{4R_ph_a}-B_{p11}\frac{h_cR_{po}G_a}{2R_ph_a}}{A_{p11}D_{p11}-B_{p11}^2}$$

$$A[10,6]=\frac{-A_{p11}\frac{h_pR_{po}G_a}{4R_p}+B_{p11}\frac{R_{po}G_a}{2R_p}}{A_{p11}D_{p11}-B_{p11}^2},\qquad A[10,7]=\frac{A_{p11}\frac{h_pR_{po}G_a}{2R_ph_a}-B_{p11}\frac{R_{po}G_a}{R_ph_a}}{A_{p11}D_{p11}-B_{p11}^2}$$

$$A[10,9]=\frac{A_{p11}\left(A_{p55}+\frac{h_p^2R_{po}G_a}{4R_ph_a}\right)-B_{p11}\frac{h_pR_{po}G_a}{2R_ph_a}}{A_{p11}D_{p11}-B_{p11}^2}$$

$$A[10,12]=\frac{A_{p11}\left(A_{p55}-F_{p12}-\frac{h_pR_{po}G_a}{4R_P}\right)+B_{p11}\left(E_{P12}+\frac{R_{po}G_a}{2R_p}\right)}{A_{p11}D_{p11}-B_{p11}^2}$$

$$A[12,5]=-\frac{R_{po}E_a}{A_{p55}R_ph_a},\qquad A[12,8]=\frac{A_{p21}}{A_{p55}R_p},\qquad A[12,10]=\frac{1}{A_{p55}}\left(\frac{B_{p21}}{R_p}-A_{p55}\right)$$

$$A[12,11]=\frac{1}{A_{p55}}\frac{R_{po}E_a}{R_ph_a}A[12,12]=\frac{1}{A_{p55}}\frac{E_{p22}}{R_p}$$

and

$$B[1,2]=B[3,4]=B[5,6]=1$$

$$B[2,3]=\frac{-B_{p11}A_{p55}}{A_{p11}D_{p11}-B_{p11}^2},\qquad B[2,6]=\frac{-D_{p11}E_{p12}-B_{p11}(A_{p55}-F_{p12})}{A_{p11}D_{p11}-B_{p11}^2}$$

$$B[4,3]=\frac{A_{p11}A_{p55}}{A_{p11}D_{p11}-B_{p11}^2},\qquad B[4,6]=\frac{A_{p11}(A_{p55}-F_{p12})+B_{p11}E_{p12}}{A_{p11}D_{p11}-B_{p11}^2}$$

$$A[6,2]=\frac{A_{p21}}{A_{p55}R_p},\qquad A[6,4]=\frac{1}{A_{p55}}\left(\frac{B_{p21}}{R_p}-A_{p55}\right),\qquad A[6,5]=\frac{E_{p22}}{A_{p55}R_p}$$

References

Adams, R.D., Peppiatt, N.A., 1977. Stress analysis of adhesive bonded tubular lap joints. Journal of Adhesion 9, 1–18.

Adams, R.D., Wake, W.C., 1984. Structural Adhesive Joints in Engineering. Elsevier, London.

Albat, A.M., Romilly, D.P., 1999. A direct linear-elastic analysis of double symmetric bonded joints and reinforcements. Composites Science and Technology 59, 1127–1137.

Anderson, G.L. et al., 1994. Embedded piezoelectric sensors to measure peel stresses in adhesive joints. Experimental Mechanics 34 (3), 194–201.

Batra, R.C., Geng, T.S., 2001. Enhancement of the dynamic buckling load for a plate by using piezoceramic actuators. Smart Materials & Structures 10, 925–933.

Chen, D., Cheng, S., 1992a. Torsional stress in tubular lap joints. International Journal of Solids and Structures 29 (7), 845–853.

Chen, D., Cheng, S., 1992b. Torsional stresses in tubular lap joints with tapered adherends. Journal of Engineering Mechanics—ASCE 118 (9), 1962–1973.

Cheng, J.Q., Taheri, F., 2005. A novel smart adhesively boned joint system. Smart Materials & Structures 14 (5), 971–981.

Cheng, J.Q., Taheri, F., 2006. A smart single-lap adhesive joint integrated with partially distributed piezoelectric patches. International Journal of Solids and Structures 43 (5), 1079–1092.

Cheng, S., Chen, D., Shi, Y.P., 1991. Analysis of adhesive-bonded joints with nonidentical adherends. Journal of Engineering Mechanics 117 (3), 605–623.

Cheng, J.Q., Qian, C.F., Zhao, M.H., Lee, S.W.R., Tong, P., Zhang, T.Y., 2000. Effects of electric fields on the bending behavior of PZT-5H piezoelectric laminates. Smart Materials & Structures 9, 824–831.

Cheng, J.Q., Wang, B., Du, S.Y., 2005a. A theoretical analysis of piezoelectric/composite laminate with larger-amplitude deflection effect, Part II: Hermite Differential Quadrature method and application. International Journal of Solids and Structures 42, 6181–6201.

Cheng, J.Q., Wang, B., Du, S.Y., 2005b. A theoretical analysis of piezoelectric/composite laminate with larger-amplitude deflection effect, Part I: Fundamental Equations. International Journal of Solids and Structures 42, 6166–6180.

Choi, J.H., Lee, D.G., 1997. Torque capacity of co-cured tubular lap joints. Journal of Composite Materials 31 (14), 1381–1396.

Chon, C.T., 1982. Analysis of tubular lap joint in torsion. Journal of Composite Materials 16, 268–283.

Crawley, E.F., de Luis, J., 1987. Use of piezoelectric actuators as elements of intelligent structures. AIAA Journal 25, 1373–1385.

Goland, M., Reissner, E., 1944. The stress in cemented joints. Journal of Applied Mechanics 11, A17–A27.

Hart-Smith, L.J., 1973. Adhesive-bonded single lap joints. NASA, CR-112236.

Hart-smith, L.J., 1983. Designing to minimize peel stresses in adhesive-bonded joints. In: Johnson, W.S., Delamination and Debonding of Materials, ASTM STP 876, 1985, pp. 238–266.

Lee, C.K., Moon, F.C., 1990. Modal sensors and actuators. Journal of Applied Mechanics 57, 434–441.

Lee, D.G., Oh, J.H., 1999. Nonlinear analysis of the torque transmission capability of adhesively bonded tubular lap joints. Journal of Adhesion 71 (1), 81–106.

Luo, Q.T., Tong, L., 2002. Exact static solutions to piezoelectric smart beams including peel stresses, I: Theoretical formulation. International Journal of Solids and Structures 39, 4677–4695.

Pugno, N., Carpinteri, A., 2003. Tubular adhesive joints under axial load. Journal of Applied Mechanics—Transactions of the ASME 70 (6), 832–839.

Roberts, T.M., 1989. Shear and normal stresses in adhesive joints. Journal of Engineering Mechanics 115 (11), 2460–2479.

Ugural, A.C., 1999. Stresses in Plates and Shells. WCB/McGraw Hill, Boston.

Wu, X.X., Cheng, J.Q., Wang, B., 2001. Influence of applied electric field on the energy release rate for cracked PZT/elastic laminates. Smart Materials & Structures 10 (5), 970–978.

Yang, C.D., 2000. Design and analysis of composite pipe joints under tensile loading. Journal of Composite Materials 34 (4), 332–349.

Yang, C.D., Huang, H., et al., 2002. Stress model of composite pipe joints under bending. Journal of Composite Materials 36 (11), 1331–1348.